THESIS FOR THE DEGREE OF LICENTIATE OF ENGINEERING

Development of Multi-grit cBN Grinding Wheel for Crankshaft Grinding

NASTJA MACEROL

Department of Industrial and Materials Science

CHALMERS UNIVERSITY OF TECHNOLOGY

Gothenburg, Sweden 2019

Development of Multi-grit cBN Grinding Wheel for Crankshaft Grinding
NASTJA MACEROL

Development of Multi-grit cBN Grinding Wheel for Crankshaft Grinding

NASTJA MACEROL

Department of Industrial and Materials Science
Chalmers University of Technology

Abstract

Crankshaft is a geometrically challenging component to grind. Over the years a number of grinding strategies have been developed to overcome thermal damage issues and excessive wheel wear. Radial and angular plunge processes have been adopted on some of the production machines. Recently a new, temperature-based strategy, has been proposed. A continuation project was launched, focusing on grinding wheel development and the initial work is presented in this thesis.

A series of grinding trails have been used to correlate the grit properties with the grinding performance. The two evaluated grit characteristics are newly proposed aspect ratio (AR) and the concentration in the grinding wheel. The results show that blockier particles (lower AR) generate high forces and lower grinding wheel wear. On the other hand, the elongated particles require less power for grinding and act more free-cutting, improving the grindability. Further trials using higher concentration grinding wheels, exhibit similar behavior as grit(s) with lower AR. The two properties that are driving this performance are the contact area between the grinding wheel and the workpiece and the undeformed maximum chip thickness h_m which changes with process and wheel design parameters.

Keywords: automotive, crankshaft, grinding, cBN, grinding wheels, vitrified bond, grit shape, morphology, aspect ratio, grit concentration

Preface

This licentiate thesis is based on the work performed at Element Six from April 2016 to August 2019. The work was carried out under supervision of Dr. Luiz Franca with co-supervision from supervisor Professor Peter Krajnik, Dr. Wayne Leahy and Dr. Radovan Drazumeric.

The thesis consists of an introductory part and the following appended papers:

Paper I: **A Methodology for the Evaluation of CBN Abrasive Grits**
Nastja Macerol, Luiz Franca, Wayne Leahy, Paul White and Peter Krajnik
Proceedings of the 19th International Symposium on Advances in Abrasive Technology, Stockholm, Sweden, 2016

Paper II: **Superabrasive Applications in Grinding of Crankshafts: A Review**
Nastja Macerol, Luiz Franca, Wayne Leahy and Peter Krajnik
Proceedings of the 20th International Symposium on Advances in Abrasive Technology, Okinawa, Japan, 2017

Paper III: **Effect of the grit shape on the performance of vitrified-bonded CBN grinding wheel**
Nastja Macerol, Luiz F.P. Franca and Peter Krajnik
Journal of Materials Processing Technology, 2019 (revision submitted)

Contents

1 Introduction

Internal combustion engines using crankshafts are still dominating in automotive and heavy duty vehicles despite the recent emergence and uncertainty regarding the electrification. However, in the light of more stringent emission regulations there is a need to improve the functional performance of key engine component through tighter geometrical and surface requirement specifications. Additionaly the cost of crankshafts are continuously decreasing. The aforementioned demands are making the manufacturing processes more challenging. The grinding process being one of the last operations holds crucial responsibility to meet these stringent demands.

Crankshafts are produced in three different ways: cast, forged or machined from billet. The former two are made to near-net shape followed by a fair amount of post-processing. The majority of high-end crankshafts, including the ones used in heavy duty vehicles are forged, machined, heat treated and ground. By not achieving the required geometrical features or surface integrity, the parts can be rejected resulting in reduced manufacturing capacity – creating significant costs and time loss to the manufacturer.

Grinding machines utilized for crankshaft grinding are specially designed to accommodate the complex geometry, particularly, the off-centre pins. Machine manufacturers utilize different strategies to grind the complex shape. In recent years researchers have tried to model the kinematics of the most widely used processes [1,2]. Consequently, they have been able to determine more and less favorable strategies. Based on the findings of Krajnik et al. [3] the authors developed and achieved/implemented a shorter process cycle by minimizing the likelihood of thermal damage.

The continuation of the process improvement done by Drazumeric et al. [2] is a project that aims to tailor and optimize the design of a special grinding wheel for crankshaft grinding application. This research includes collaboration of the whole technology value chain, from grain and wheel manufacturer to end user.

The research focus, reported in this thesis, is an evaluation of the effects on grinding when changing wheel design parameters, specifically:

    (i) cBN grit properties
    (ii) grit concentration

Currently the wheel designs are customized by the wheel manufacturers, keeping it their know-how. The common knowledge is that the end users mostly grind with vitrified bonded wheels containing a high concentration of relatively strong cubic boron nitride (cBN) grains.

2 Grinding process

Grinding is a machining operation where the cutting points are geometrically undefined abrasive grains stochastically distributed in the grinding tool. Grinding is traditionally considered as a finishing process where the surface requirements are high. A significant amount of grinding operations are also heavy-duty where the objective is to remove material as quickly and efficiently as possible, with little focus on surface finish [4].

There are a number of different kinematic set-ups that enable the grinding of different workpiece geometries (e.g. cylindrical, surface, face, double-disc grinding). Nevertheless, a number of basic components aremandatory for the process to run: (i) a grinding wheel, (ii) a workpiece material, (iii) at least one coolant nozzle pointed at the grinding zone, and in most cases (iv) a dressing tool used to sharpen the wheel when necessary (Figure 1).
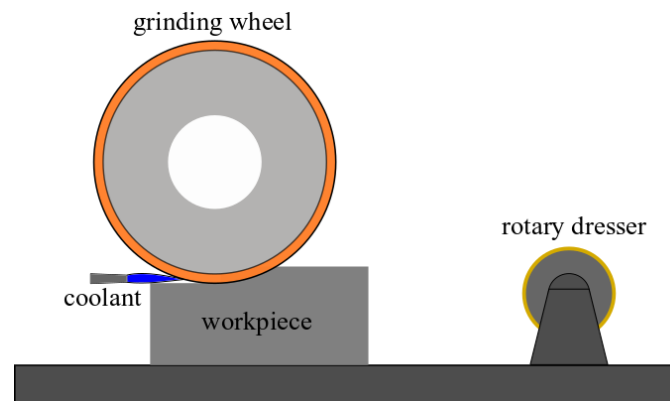

Figure 1: Grinding set up including the mandatory components.

2.1 Crankshaft grinding processes (Paper II)

Specially designed machines are used to grind complex geometry of a crankshaft. Some of the main builders of s machines are: Jtekt Corporation, Fives Landis Ltd. and Junker Group. The challenges they encounter when designing them are:

1. Off-center crankpin journals (Figure 2)

2. Complex profile geometry of a crankpin that consists of bearing surface, sidewall and radius connecting the two (Figure 2)
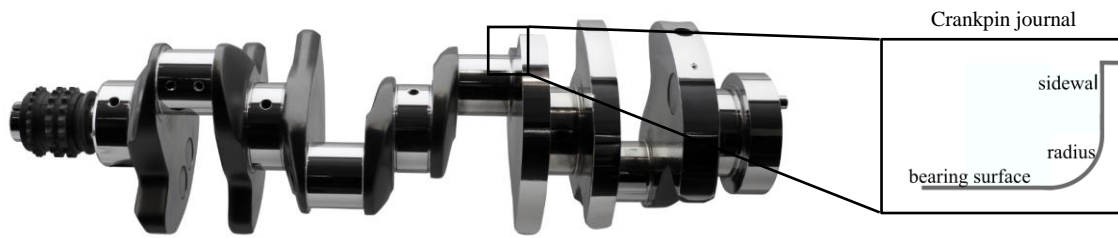
Figure 2: Crankshaft with highlighted pin journal and its geometrical features (Reprinted with permission of Element Six).

A fair amount of patents proposing new strategies to grind crankpins have been published over the years, the majority of them by machine builders who have embedded these strategies into the machines NC control. This saves the end users a lot of time because they do not have to develop their own processes. It has been also mentioned, [5] that the freedom to change the existing programs is also limited leading to fewer improvement possibilities.

One of the first patents on crankpin grinding (published in 1986) attempts to improve the plunge grinding proces [6]. This is the first proposed angle plunge grinding process (Figure 3) .
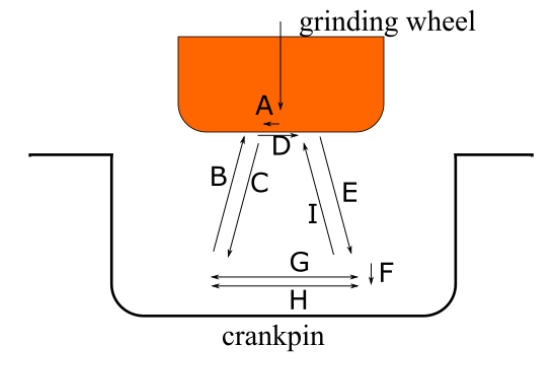

Figure 3: First proposed angle plunge grinding method (Adapted and modified from [6]).

Cinetic Landis Grinding Limited published an improved angle plunge grinding method in 2008 [7]. The patent claims that the rubbing (of grits over a workpiece) is reduced through improved control of feed rates, dwells, workpiece speeds and coolant pressure/flow in each step.

In 2006, a patent was filed by Toyoda Koki Kabushiki Kaisha (Figure 4) proposing a novel method to reduce contact between the workpiece and the grinding wheel in order to improve swarf removal and reduce the likelihood of wheel loading [8].

4
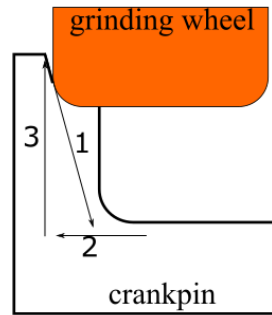
Figure 4: Novel grinding method developed by Toyoda Koki Kabushiki Kaisha (Adapted and modified from [8]*).*

An alternative approach to grinding a crankshaft has been proposed by JTEKT Corporation (Figure 5) where the wheel shuttles between the sidewalls, allowing the coolant to reach previously ground zones when the wheel is not in contact with the workpiece [9].
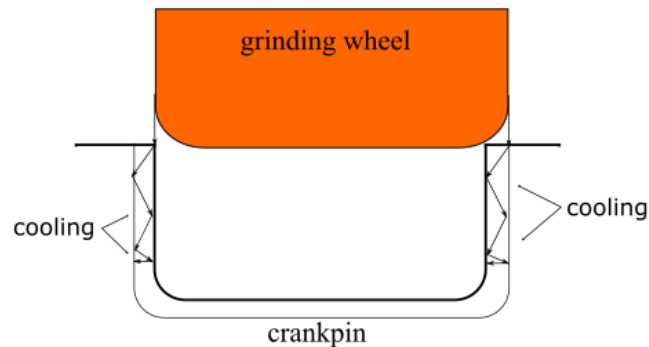
Figure 5: Alternative approach to grinding a crankshaft proposed by JTEKT (Adapted and modified from [9]*).*

Oliveira et al. [1] compared two commonly used grinding strategies for sidewall grinding where the likelihood of thermal damage is higher: (i) axial plunge and (ii) axial face grinding. As a result they proposed an improved multi-step approach, where multiple axial grinding cycles are made at different radial positions to remove the material on the sidewall (Figure 6). The process appears very similar to angular plunge grinding [10].
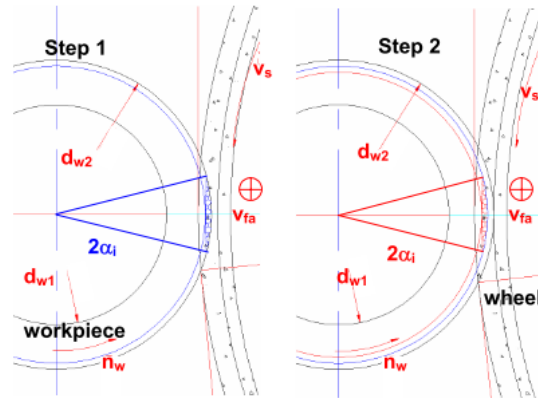
Figure 6: Multi-step grinding strategy (Reprinted from CIRP Annals- Manufacturing Technology, 54/2, J. F. G. Oliveira, E. J. Silva, J. J. F. Gomes, F. Klocke, D. Friedrich, Analysis of Grinding Strategies Applied to Crankshaft Manufacturing, 269-272, Copyright (2005), with permission from Elsevier).

Researchers modelled the wear of the grinding wheel for the three grinding strategies (Figure 7) and were able to determine the most affected parts. Axial plunge grinding (strategy A) has exhibited the lowest dressing interval due to excessive wear on the radius. On the other hand, the multi-step axial strategy (strategy C) allows the highest amount of parts being ground before redress. The reason is the flexibility of changing the number of steps and thus manipulating the wheel wear.
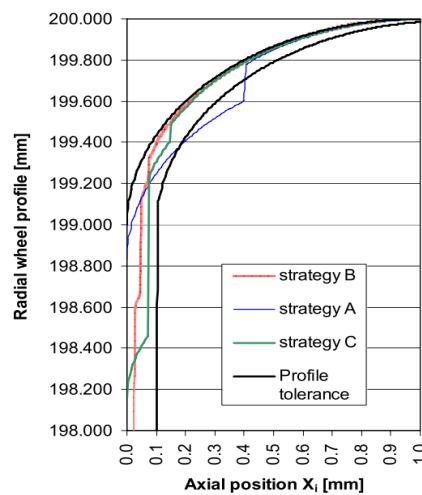

Figure 7: Wheel wear profiles for different grinding strategies (Reprinted from CIRP Annals-Manufacturing Technology, 54/2, J. F. G. Oliveira, E. J. Silva, J. J. F. Gomes, F. Klocke, D. Friedrich, Analysis of Grinding Strategies Applied to Crankshaft Manufacturing, 269-272, Copyright (2005), with permission from Elsevier).

6

2.1.1 Temperature based method of grinding a crankshaft

The geometry and kinematics of plunge and angle grinding strategies were modelled by Drazumeric et al. [2]. They described incremental changes of fundamental grinding parameters at each point of the crankpin profile and throughout the entire grinding cycle. Figure 8 shows variation of the specific material removal rate Q' when grinding a crankshaft using two different strategies. A surge in Q' can be observed at the end of the radial plunge grinding cycle. This phenomenon increases the likelihood of thermal damage. Equally, excessive wheel wear, on the portion of the wheel subjected to the most aggressive grinding conditions, is unavoidable. On the other hand, the angle plunge grinding strategy shows improvement by reducing the Q' variation hence a shorter grinding cycle time.
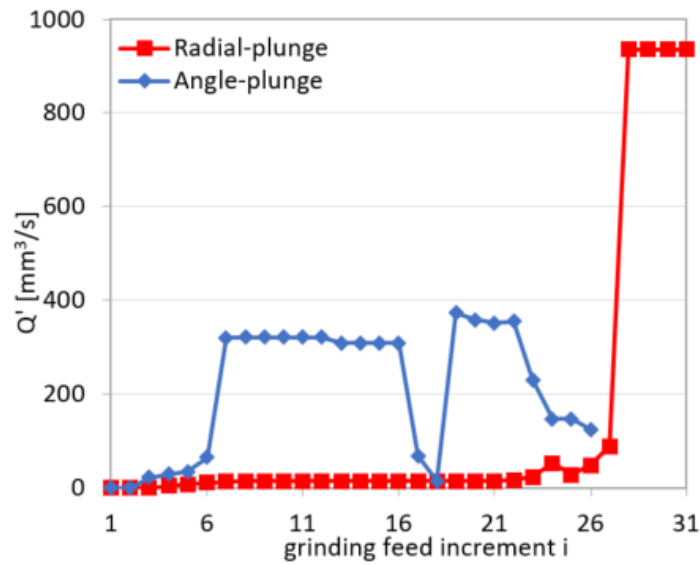

Figure 8: Changes in Q' for two different grinding strategies throughout the process (Adapted and modified from [11]).

A new grinding strategy was developed in the light of analysis [3]. Researchers utilised Jaeger's moving heat-source model [12] to define parts of the wheel that generate most heat (Figure 9). Consequently, each grinding increment is calculated/determined in a way that the critical points on the wheel stay below or at a set maximum surface temperature of the workpiece according to the following formula:

$$\theta_m = 1.064/(k\rho c_p)^{\frac{1}{2}} e_w aggr(s) Q'(s)/(l_c(s)v_w)$$

where θ_m is the maximum surface temperature, k is material thermal conductivity, ρ is its density c_p is specific heat capacity , l_c describes the contact length between the workpiece and the wheel, v_w is the workpiece speed, $Q'(s)$ is the specific material removal rate at an arbitrary

point on the grinding wheel profile, e_w is the specific grinding energy into the workpiece, which depends on aggressiveness and can be experimentally determined [2]. Aggressiveness ($aggr(s)$) is a non-dimensional parameter [13] and is calculated for any position on the grinding wheel profile [2].
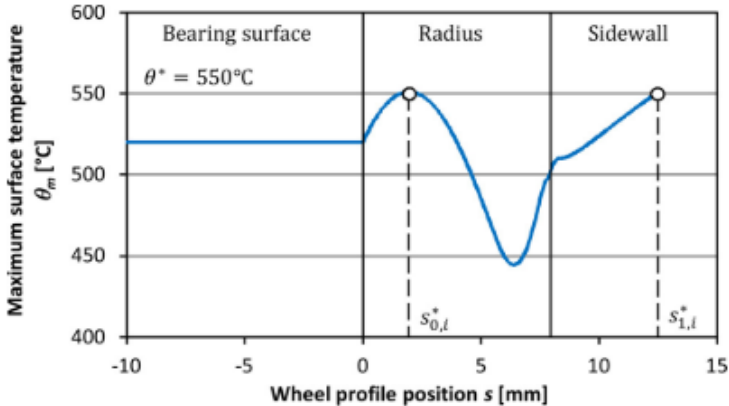

Figure 9: Maximum surface temperature along the wheel profile (Reprinted from Journal of Materials Processing Technology, 259, Radovan Drazumeric, Roope Roininen, Jeffrey Badger, Peter Krajnik, Temperature-based method for determination of feed increments in crankshaft grinding, 228-234, Copyright (2018), with permission from Elsevier)

Figure 10 shows a comparison of the newly developed and the well-established crankshaft grinding strategies. Notice a significant reduction in cycle time by running a grinding process on a burn threshold – maximizing grinding performance to the allowable limits.
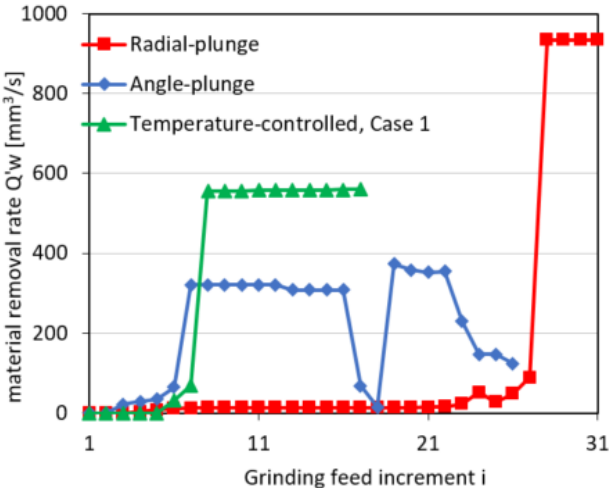

Figure 10: Two examples of temperature controlled strategy in comparison to standard processes (Adapted and modified from [11]).

The above-described method is the base for the wheel optimization project concerned here. It gives valuable information regarding the variation of fundamental grinding parameters during

8

the most affected stages of the process cycle (i.e. Q', l_c, $aggr$, θ). The findings are crucial for interpretation of the abrasive-grit trials presented in this report and for proposing further work.

2.2 Grinding wheel

The grinding wheel is a crucial part of the grinding system. Its major task is to remove the workpiece material in order to obtain a required geometry and surface integrity. The most obvious difference in comparison with turning and milling tools is the undefined geometry of cutting edges, stochastically distributed on the surface of the grinding wheel.

A number of grinding wheels are available on the market. Two possible classifications are summarized in the Figure 11.
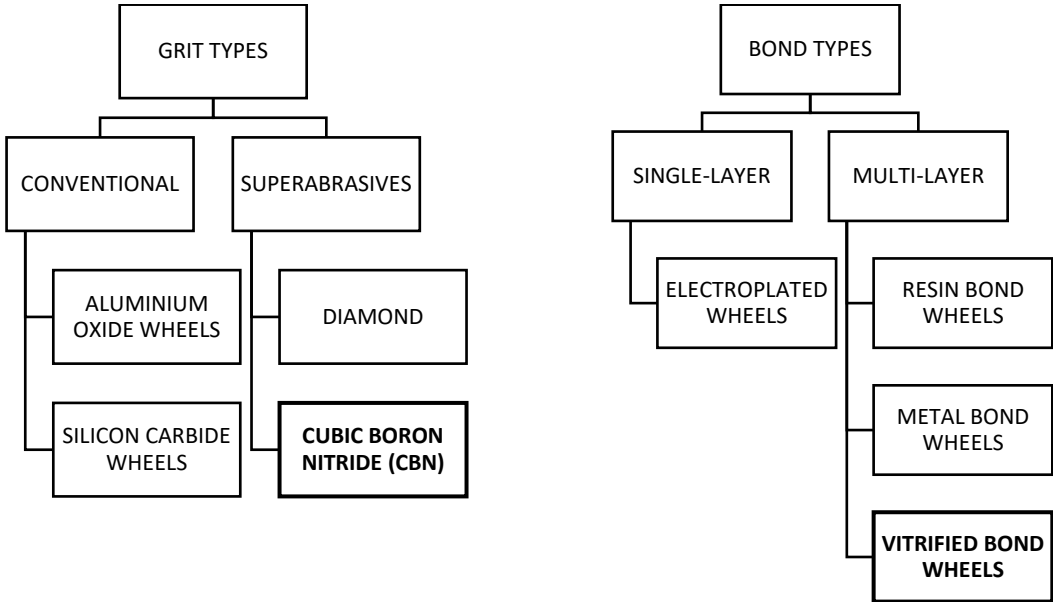
Figure 11: Grinding wheel classification possibilities.

A vitrified bonded cBN wheel is the most commonly utilized tool in crankshaft grinding applications, particularly in finishing operations. In roughing operations electroplated tools have proven to be very effective, achieving Q' of up to 2000 mm³/mms [14].

Superabrasive wheels substituted conventional wheels due to increased productivity and tool life, especially in large-volume production with severe conditions [15]. They are normally made of a hub, using different materials (e.g. steel, carbon fiber reinforced plastic (CFRP)) and approximately a 3-5 millimetre thick layer of the abrasive mixture (i.e. bond, grit and porosity) [16]. A well designed abrasive layer gives the tool high elastic modulus, low fracture toughness, good thermal stability and high rigidity. A combination of the superior properties of all the

aforementioned components protects the wheel against excessive wear and chemical attack from the grinding fluid (coolant). Additionally, it allows the wheel to withstand high grinding and centrifugal forces and high grinding temperatures.

2.2.1 Bond system: vitrified

The crucial attribute of the vitrified bond is the sufficient bulk strength to overcome stresses caused by high peripheral speed of an operating wheel. The same property also enables sufficient holding force of the cBN grits during the grinding process. The grinding process will not be efficient or will even fail if these basic requirements are not met. While the bond has to have sufficient strength, it also has to be able to fracture, preferably in a controlled manner, in order to maintain the sharpness of the wheel for longer periods. Fluidity is another important parameter, which can improve the adhesion between the grit and the bond. The two properties can be altered by modifying the bond composition and heat treatment process. A significant proportion of published literature is focusing on the effects of composition on the mechanical properties.

Yang et al. [17] evaluated the bond strength by adding a number of different materials (e.g. Al_2O_3, B_2O_3). They found that some of them minimize the thermal expansion coefficient mismatch between the grain and the bond, increasing the strength. A similar observation was reported when adding a specific amount of TiO_2 [18]. Adding this material to the bond also reduced fluidity, minimizing the porosity and increasing the strength. Similar results were achieved using $LiAlSi_2O$ and $LiAlSi_3O_8$ [19]. Wang et al. [20] used ZrO_2 in view of reducing fluidity and improving the distribution of porosity which in turn increases the bond strength due to the improved adhesion of grit with the bond.

2.2.2 Porosity

Porosity has several extremely important roles. Firstly, it gives the coolant the space to flow and in return transfers the heat from the grinding zone. Secondly, it provides the needed clearance for the grinding chips during the process [21]. Considering it is an open, material-free space, it automatically reduces the friction and the heat generation between the workpiece and the wheel (rubbing action). Carefully designed pores can also reduce the crack propagation, and consequently, increase the impact strength of vitrified bonded tools [22].

10

There are three main ways of introducing porosity into the vitrified bond wheel. The first, simplest way is to add pore former to the green body and let it burn off during sintering. This material is normally a carbon-based material such as phenol resin and amorphous carbon [23]. Mao et al. [24] successfully used granulated sugar as a filler as it is readily available in different particle sizes and in large quantities. Similar results can be obtained also by using nut shells or PMMA (polymethylmethacrylate) microspheres [25]. The disadvantages with the aforementioned pore formers is that they can be challenging to remove and can thus form defects on the product due to swelling. In order to reduce the challenges with conventional pore formers the second option has been developed where liquid CO_2 is used as a solvent to remove pore inducers [26]. The third group of pore formers are ceramic materials designed as hollow shells, e.g. alumina bubble particles [27]. They form enclosed pores that fracture and open during the grinding process.

It is important to emphasize the importance of pores in vitrified bonded wheels. It is equally important to understand that poorly designed, e.g. too high amount of porosity can lead to inadequate performance. For these reason is it crucial to understand the requirements and challenges of the application and the grinding kinematics.

2.2.3   Abrasive grits: cubic Boron Nitride (cBN)

There are two main abrasive families: (i) conventional and (ii) superabrasive. The former can be further divided into aluminum oxide (Al_2O_3) and silicon carbide (SiC) and the latter to diamond and cBN. Conventional abrasives dominated all grinding operations until superabrasives emerged. New learnings were crucial (e.g. wheel design, grinding process and machine design) to obtain the benefits of a significantly stronger grit. Since then the grinding wheel technology and machine designs have improved significantly. Nowadays it is very common to see superabrasives being used in the grinding industry. cBN is particularly successful in ferrous grinding applications due to its chemical inertness in such environment as well as high thermal stability. Diamond on the other hand is a superior choice when grinding ceramics, glasses and cermet materials especially due to its hardness. The downside of diamond is that it deteriorates rapidly at elevated temperatures through graphitization and oxidation [28], particularly in the presence of catalysts that are normally present in ferrous materials [4].

The first cBN synthesis was reported in 1956 [28]. The use in industrial grinding only started in the 1980s, early 1990s [15]. cBN is a transformation of hexagonal boron nitride to cubic

boron nitride with the diamond lattice structure made up of boron and nitrogen atoms (Figure 12). In his patent, Wentorf [28], describes using boron or boron nitride in the presence of at least one catalyst to transform hBN to cBN at high pressures and high temperatures (HPHT). Based on experimentation he was able to develop a phase diagram for cBN synthesis.
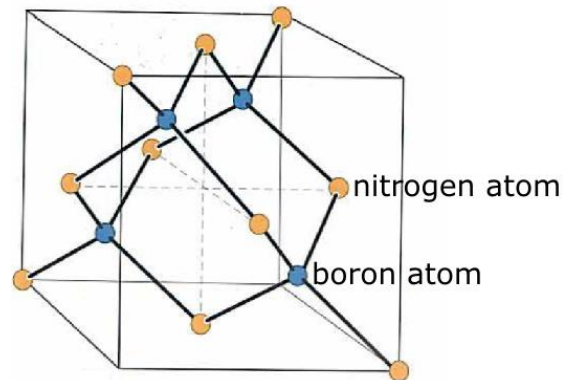
Figure 12: cBN lattice structure (Reprinted from Material synthesis- internal report, G. Davies, Copyright (2014), with permission from Element Six).

Very little research is reported after the initial cBN development work. Only in the 1990s and especially in the 2010s did scientists become more interested in this topic. At the time cBN grades started to emerge at the market from major manufacturers [29] as well. However, the synthesis and material properties details were mostly kept as proprietary knowledge.

There are two main ways of manufacturing grits with different properties: using different materials (chemistry) in synthesis and changing the process parameters. Each of the two can be further divided into several subcategories (e.g., pressure, temperature, time, solvent choice, seeding and spontaneous nucleation), generating numerous combinations. Nevertheless, there are process boundaries dependent on the choice of the material to be synthesized and the process parameters [30].

The intrinsic nature of cBN crystal is colorless [31], even though the majority of commercially available materials are brown, amber or black. The latter is a result of different impurities and defects introduced by solvents and additives.

Taniguchi focused his research on synthesis of high purity large cBN grits with the aim of utilizing the electrical and optical properties. Together with Yamaoka [32], they reported a successful synthesis of large colorless (using barium boron nitride solvent) and amber crystals (using lithium boron nitride solvent) through spontaneous nucleation. They discovered that the latter contain significantly higher amounts of oxygen – suggesting this element is an important

source of impurity in obtaining particular type of material. Beryllium doped cBN crystals were grown in lithium boron nitride and calcium boron nitride solvent systems, resulting in dark blue color cBN exhibiting a type of semiconducting characteristics [33]. Growing cBN in a barium boron nitride solvent system produced very low oxygen and high purity crystals [34].

Several other solvents were utilized in synthesis processes with the aim to improve crystallinity, purity or yield or to increase the growth region on $p - T$ diagram. Kubota and Taniguchi [35] developed a cBN phase diagram using metal alloy solvent, i.e. nickel molybdenum. Chinese researchers proved that by adding lithium fluoride, crystal can change from irregular and yellow to transparent and crystalline [36]. Poor crystallinity cBN were grown by a number of catalysts (e.g. lithium, calcium or manganese) [37]. By adding boron to lithium nitride system, well-shaped and pure particles, were obtained, containing less residual stress than their yellow counterparts.

A high proportion of research was aimed to grow large, high purity and good crystallinity particles for optical and electrical analysis purposes. The mechanical properties of grit are normally not reported as part of the new synthesis processes but as part of grinding trials [38,39]. The reason could be that the equipment known and used by grit manufacturers was not available to the research groups that were synthesizing alternative cBN materials.

The most common cBN product on the market is monocrystalline although a small number of polycrystalline types are available as well. Some of them have limited use due to excessive strength, which limits the fracture mechanism during grinding. As a result, the grit dulls, and generates heat leading to thermal damage. Polycrystalline cBN and similar materials have recently been researched more frequently (e.g. ultrafine polycrystalline cBN [39], aggregated cBN (AcBN) [40], polycrystalline cBN (PcBN) [41,42]). Researchers claim that their main advantage is better self-sharpening and more controlled fracturing that prolongs the tool life.

2.2.4 cBN properties

General properties of cBN such as strength, thermal stability, heat conductivity and chemical inertness are the major reasons why cBN is widely used in grinding operations. The majority of properties are challenging to measure but a limited number were developed to the point they became quality control parameters and grit differentiators.

The most established measurable cBN property used is the impact strength value or Toughness Index (TI) from the Friability Impact (FI) tester developed by Belling and Dyer [43]. The purpose of measuring TI originates from diamond due to the necessity for monitoring the quality (or strength) of synthesized products. FI has now been commonly used to differentiate cBN products as well to help track the quality and to allow the determination of the most suitable superabrasive product for a particular application.

Color being the consequence of impurities developed by solvents and additives is also a relatively important microstructural property as it gives the initial direction for use. The bond and grinding application can be determined by a simple visual evaluation of color. Amber materials (e.g. ABN900) are well known to be used in electroplated tools and brown materials are believed to perform the best in vitrified bonded tools (e.g. ABN800). Black materials are often regarded as inferior materials used in resin bond and lower strength vitrified bond wheels. Color can be measured using a spectrophotometer, but no research can be found to better understand the effects it has on the mechanical or geometrical surface properties.

The physical shape of the grit is becoming a more important parameter, not only for grit size between 0 to 50 μm (Element Six product in this range is Micron +MDA) but also in grit for grinding wheels. In smaller grit-size products, it is paramount to have uniform shape in order to ensure high quality surface finish (e.g. wafers for semiconductors). cBN manufacturer still frequently use descriptive adjectives to describe the shape of the grit (e.g. elongated or blockier). There are commercially available measuring devices that can evaluate grit shape. Camsizer by Retsch Technology uses dual camera system to capture larger and smaller particles. Using mathematical algorithms it is able to provide a range of parameters about the grit (e.g. 2D aspect ratio, length, diameter and others). It is up to a user to choose the most relevant ones. An established parameter describing the relationship between the width (w) and the length (l) of an image projection of the particle is aspect ratio: $AR = l/w$ (Figure 13).
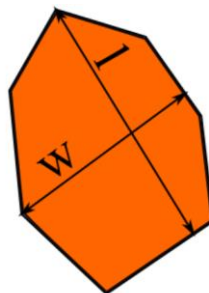
Figure 13: AR determined by length and width of a grit particle.

The challenge with the majority of measuring techniques is the fact that they can only evaluate two dimensional shapes. This means that a particle can have a width to length ratio close to 1 but the thickness is very small – e.g. platelet-like grit (Figure 14, a). On the other hand, the grit can have all three dimensions in a proportional range (Figure 14, b). The performance of the two in the grinding wheel can be significantly different.

a)   b)

Figure 14: Different 3D shapes of particles: a) platelet-like and b) octahedron.

Chen et al. [44] recently introduced an alternative set of grit shapes based on 3D geometries. They claim that each grit sample consists of a limited number of different geometries that should be considered when evaluating the grinding performance. Using just one simplified parameter is not sufficient.

Shape and morphology are sometimes used in the same context, however they explain different cBN attributes. Morphology focuses on the growth characteristics rather than just physical shape of crystals [45]. It is more complex for cBN than for diamond due to structural symmetry loss and fractured surfaces. The morphologies of Element Six commercially available products are presented in Figure 15.
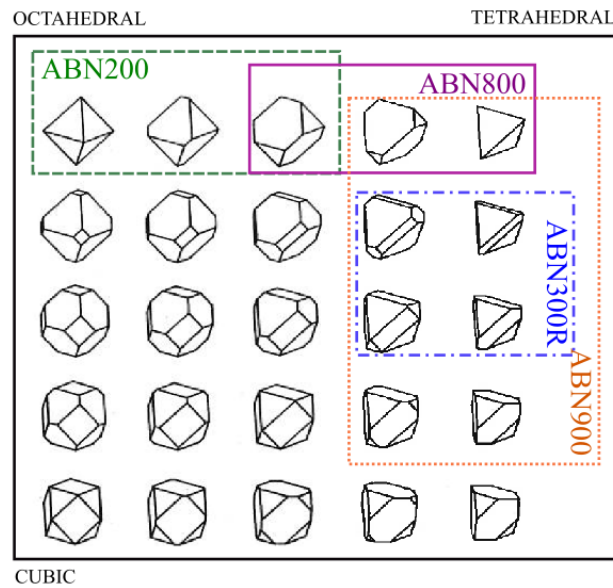
Figure 15: Morphologies of Element Six cBN grades (Adopted and modified with permission of Element Six).

2.3 Application: effect of cBN properties on grinding performance

Initially, when cBN was developed, the vitrified bonds were not strong enough to hold the grit adequately, resulting in poor performance. Hitchiner and McSpaden [46] reported grinding results exhibiting higher wheel wear when using tougher girt. They attributed this phenomena to a weaker bond. Additionally, they mentioned the possible effect of shape or morphology of the grit on the grinding results. Similar observations were done by Upadhyaya and Fiecoat [47] when they tested grit with the same strength and obtained different performance.

A very important property of the grit is adhesion with the bonding material. Naturally both material belong to the same family making them compatible. That is also the reason why cBN grit is normally not coated when used in vitrified bonded tools [48]. Jackson et al. [49] analyzed the interaction between the cBN surface and the bond. They observed a boric oxide layer that grows with increased sintering temperature. At the saturation point the thickness remains constant regardless of the temperature. As a result of boric oxide layer thickening, the tool life increases as shown in Figure 16. Wheel life is expressed as G-Ratio (the higher the G-Ratio the lower the wheel wear and vice-versa) that increases with the bond content and temperatures.
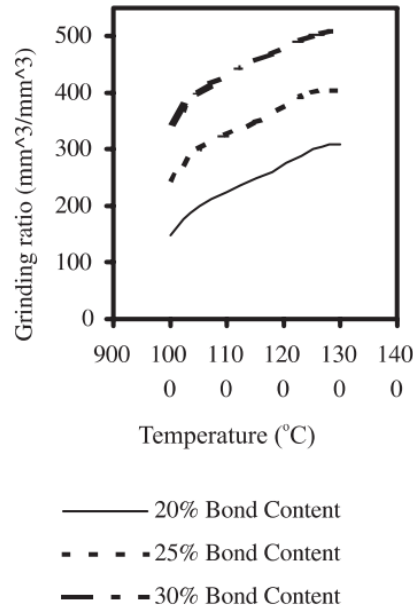
Figure 16: Grinding ratio changes with sintering temperature (Reprinted by permission from Springer Nature Customer Service Centre GmbH: Springer India, Academy Proceedings in Engineering Science, [49]*, Controlled wear of vitrified abrasive materials for precision grinding applications, M. J. Jackson, BB. Mills, M. P. Hitchiner, Copyright (2003)).*

General wear stages of cBN grinding wheels are relevant for all grit types regardless of their properties. The three main wear modes are summarized below:

1. Abrasive or attritious wear is dulling of grit. In well-designed grinding process this type of wear is not common but is still very important to be monitored. Grit dulling can quickly increase heat generation and thermally damage the workpiece [50].

2. Fracture wear, particularly controlled fracture, of cBN is the most desirable mode. It enables self-sharpening of the grinding wheel, and consequently, prolongs its life. The grain fracture rate manifests itself in grinding forces and the grinding wheel wear rate [51].

3. Bond fracture or fracture of interface between the bond and the grit. The former can be recognized as fast, excessive, wheel wear. It could also suggests that particular bond is too weak for the chosen grit type [46]. The interface fracture is difficult to evaluate. Normally, cBN and bond are compatible. Nevertheless, when grit surface is not adequately prepared, the adhesion strength can be compromised. Equally, if the bond is not designed well, it can reduce wetting around the grit, reducing the holding properties.

Fracture wear of grit can be further divided in micro and macro wear. The former is believed to be typical for polycrystalline cBN materials [39] and the latter for monocrystalline. Bailey and

17

Juchem reported the differences observed amongst the monocrystalline materials. Their experiments showed that the fragment size is determined by growth characteristics which in turn affects grinding behavior [52].

In recent years, wear mechanisms have been often researched by means of a single grit tests [53]. Valuable knowledge can be gained by evaluating individual particles [54–56]. On the other hand, the wear can be greatly affected by the geometrical features, grinding parameters and machine accuracy and stability. A correlation between the single grain wear and the grinding wheel wear is not established yet, due to uncertain (wear) contribution of the bond.

3 Research methodology: experimental investigation

Two sets of grinding trials were conducted with the aim of evaluating the process outputs when using different grit types and concentrations. Initially, the grit analysis techniques are described followed by the detailed explanation of grinding set up and types of tests. The grinding model used for analysis of grinding forces, power and specific grinding energy is briefly introduced in chapter 3.3.

3.1 cBN characterization

Two main parameters evaluated for all tested grits are: (i) strength and (ii) aspect ratio. The strength was tested using internal standard procedure [57] based on Belling and Dyer [43]. A defined carat weight is being fractured with a specified number of cycles using a vibratory device. Finally, the weight of more and less fractured particles is compared. The materials that fracture more are considered to have lower strength and vice-versa.

The second parameter, measured by dynamic-image analyzer (Camsizer XT), is the aspect ratio (AR) indicating the physical shape of the grains (details in chapter 2.2.4). 20,000 images were taken and from three samples of each grit type according to ISO 13322-2.

3.2 Experimental set-up (Paper I)

Grinding trials were conducted on a Blohm (MT408) surface grinding machine at Element Six. The set-up is shown in Figure 17. Kistler dynamometer (Type 9257A) was used to measure grinding forces in situ. Two high pressure nozzles were ensuring the wheel was continuously cleaned and the process cooled. The high pressure nozzle was pointing at the top of the wheel with 5MPa (50 bar) while the lower pressure nozzle was pointing to the grinding zone at 0.9 MPa (9 bar). An emulsion of synthetic polymer lubricant and corrosion inhibitors (HoCut 768), in a concentration between 4.5% and 5% was used as the coolant in all trials. The workpiece material was bearing steel 100Cr6 with hardness of 61±1 HRC.
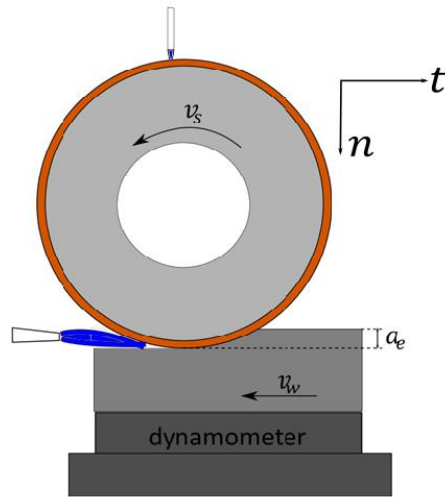
Figure 17: Grinding set up.

The methodology consists of two types of grinding tests:

1. Window of operation test where the grinding efficiency of grinding wheel is tested over a wide range of grinding parameters by changing the Q' in particular. The grinding wheel is initially dressed followed by a number of (no-dress) grinding passes with the aim to stabilize the grinding force and eliminate dressing effect [58]. Once the process is stabilized, Q' is varied by changing the v_w (workpiece speed) and the a_e (depth of cut). The number of passes per each set of grinding parameters is minimized in order to avoid grinding wheel wear.

2. Micro wear test focuses on grinding wheel wear at a specific Q'. A set workpiece volume is ground utilizing only half of the grinding wheel. A groove is generated on the grinding wheel enabling wheel wear measurements (also commonly known as a razor-blade technique). The wear in a shape of a step is measured using an optical 3D surface measurement system (Alicona G5). Surface roughness is evaluated using a tactile surface-roughness tester (Taylor Hobson Surtronic S-100). Gaussian filtering is applied with a cut-off length of λ = 0.8 mm.

The dressing parameters are kept constant for both test types (Table 1). It is important to note that dressing is performed only at the start of the window of operation and the micro wear tests. There is no dressing between the passes.

Table 1: Dressing parameters.

Overlap ratio, U_d	4
Depth of dress, a_d	0.003 mm
Wheel-dresser speed ratio, q	0.81

3.3 A method for analyzing grinding data (Paper III)

The maximum undeformed chip thickness h_m is the key input parameter that defines the grinding process. It can be controlled by process parameters (v_w, a_e, v_s, l_c) and grinding wheel design parameters (l_c, C, r) and can be expressed as follows [59]:

$$h_m = ((4v_w a_e)/(Crv_s l_c))^{1/2} \qquad (3.1)$$

where C is a number of active grits per unit of wheel surface, r is the chip width-to-thickness ratio and $l_c = (a_e d_{eq})^{1/2}$ is the wheel-workpiece contact length, and d_{eq} is the equivalent wheel diameter. Determining h_m is very challenging, particularly the wheel design parameters C and r. They are often determined arbitrarily and considered as a constant. Vinay and Rao [60] and Agarwal and Venkateswara Rao [59] have reported formulas that can help calculate C and r. Proposed formulas require a certain level of assumptions. For example, a number of active particles on the surface has to be estimated unless a very lengthy evaluation of grinding wheels is carried out. This process can be relatively subjective in the case of a vitrified bonded wheel. Notice, h_m is not only varied through process but also through the wheel design. Some of the generated grinding results are presented as a function of input parameter Q' and h_m.

The output of the grinding process is analyzed using well-known grinding parameter relationships. The contribution to the specific energy in grinding (i.e. energy per unit volume of material removal) consists of three independent mechanisms that are taking place at the wheel-workpiece interface [50]: (i) cutting or shearing, (ii) ploughing or plastic displacement and (iii) frictional, sliding or rubbing contact along the grit and bond wear flats. Considering that the ploughing component is negligible when the grinding wheel is engaged with the workpieces at sufficient depth of cut, generating chipping [61], the force F acting on the grinding wheel at any given point are a sum of two components [50]:

$$F = F_c + F_f \qquad (3.2)$$

where F_c (N) is the cutting or shearing component and F_f (N) is the friction or rubbing component (grits wear flat and bond bearing surface). The normal F_n and the tangential F_t components of the total force can be expressed as:

$$F^n = F_c^n + F_f^n \qquad (3.3)$$

$$F^t = F_c^t + F_f^t \qquad (3.4)$$

Assuming the process is ductile, the cutting component of the force can be further decomposed as follows [50,62]:

$$F_c^n = \xi u_e^* a_c \qquad (3.5)$$

$$F_c^t = u_e^* a_c \qquad (3.6)$$

where u_e^* (J/mm^3) represents the intrinsic cutting specific grinding energy, corresponding to the lowest energy used to remove a unit volume of workpiece using a perfectly sharp wheel [4], and ξ defines the inclination of the cutting force [62].

Following the frictional relation $F_f^t = \mu F_f^n$ and combining it with Eq. (3.3 - 3.6), a following relationship can be obtained:

$$P^{t\prime} = u_e^* Q' + P_f^{t\prime} \qquad (3.7)$$

where $Q' = a_e v_w / w$ (mm^3/mms), w being the wheel width in contact with the workpiece and $P_f^{t\prime} = F_f^{t\prime} v_s / w$. The latter parameter is called threshold power and is illustrated in Figure 18. The linear relationship between power and material removal rate is only valid when $Q' \geq Q'_{min}$. In the opposite case, when, $Q' < Q'_{min}$, rubbing and ploughing are dominating and the response is characterized by a nonlinear relationship between $P^{t\prime}$ and Q' [58]. Similarly, when, $Q' > Q'_{max}$, an alternative model is required due to brittle cutting mode.
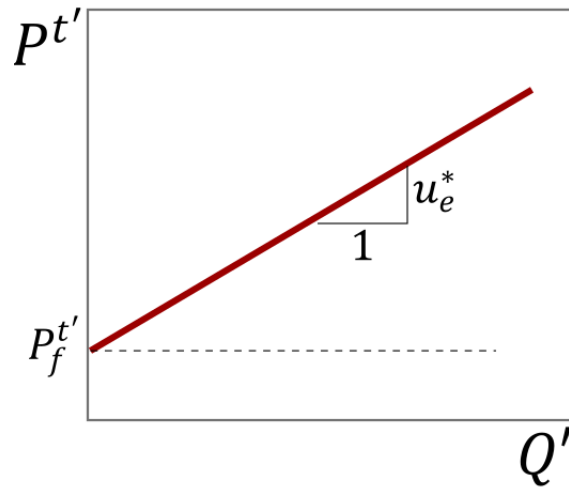

Figure 18: Correlation between the power ($P^{t\prime}$) and material removal rate (Q').

3.4   Experimental results

The temperature-based crankshaft-grinding strategy developed by Krajnik et al. [3] and its requirements [2] are the base for the research of the effects of grit properties on the the grinding process. The following two components of the wheel design have been evaluated:

  (i) Aspect ratio of grits (Paper III) and

  (ii) Concentration of grits

3.4.1   Grit aspect ratio performance evaluation (Paper III)

In Paper III monocrystalline grits (Grit A – Grit D) with different geometrical features were evaluated and tested in grinding trials. Their effects was compared in terms of grinding efficiency and wheel life. Out of seven different grit types, three (Grit A, Grit D and Grit F) came from the same chemistry and synthesis process. They were post processed in order to achieve the desired shape. The other three, came from a different synthesis processes (Grit B, Grit C and Grit E). The size of all grit was mesh 120140 with the average grain size of 126 μm.

The strength of grit samples was measured, and is compared as illustrated in Figure 19. The shape, on the other hand, changes radically from one grit type to another, as can be seen on the y-axis. Notice, that the synthesis output is not necessarily strength variation but also shape.
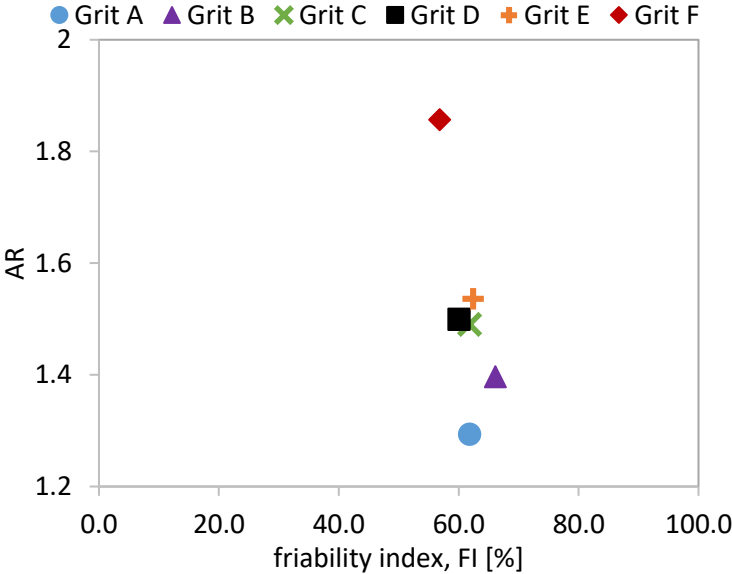

Figure 19: Tested grit properties.

Six grinding wheels, containing the same amount of bond, porosity and grit (concentration is C150=6.6ct/cm^3), were prepared for testing. The potential variables of the wheel manufacturing process were not considered in the trials. As mentioned previously, h_m changes with the wheel

design modifications based on grit AR. For the purpose of calculating h_m following assumptions were made: (i) half of the particles on the wheel surface are engaged during grinding process and (ii) r is calculated based on the aspect ratio of grit particles [60].

The grinding parameters used in trials are summarized in Table 2. The reason for the choice of parameters is to have small contact length and relatively large h_m – common occurrence in cylindrical and surface grinding. The relatively high concentration of the grit in the wheel is also more suitable for such applications.

Table 2: Grinding parameters for window of operation test.

Wheel speed, v_s	40 m/s
Depth of cut, a_e	0.01 - 0.3 mm
Workpiece feed rate, v_w	1.2 - 24.6 m/min
Specific material removal rate, Q'	0.6 - 33 mm^3/mms

The results of the window of operation trials are shown in Figure 20. Notice, that the inclination of the trend lines is similar for all tested grits. This suggests that changing the grit shape, particularly the aspect ratio, does not affect u_e^* significantly. The lowest energy to cut a volume of 100Cr6 using this particular wheel type is constant regardless of the grit shape.
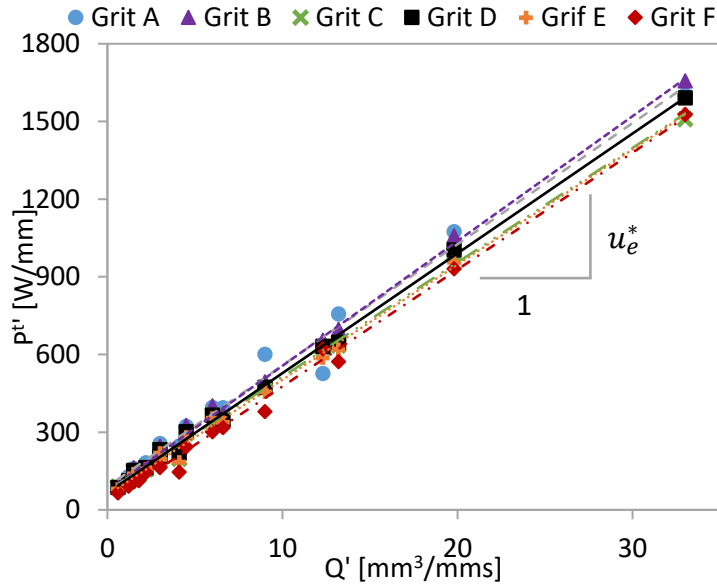

Figure 20: Window of operation results for Grit A to Grit D.

Specific threshold power ($P_f^{t\prime}$) values are measured as illustrated in Figure 18. The results suggest that at particular Q' the total $P^{t\prime}$ varies with grit shape, affecting $P_f^{t\prime}$. The correlation

24

between the $P_f^{t'}$ and AR is illustrated in Figure 21. The reason can be the differences in contact area between the wheel and the workpiece. Some of the preliminary correlations between the wheel bearing area and threshold power measurements were reported in Paper III. The images of the wheels suggest that grit with lower AR (blockier) has higher contact area comparing to the grit with lower AR (elongated).
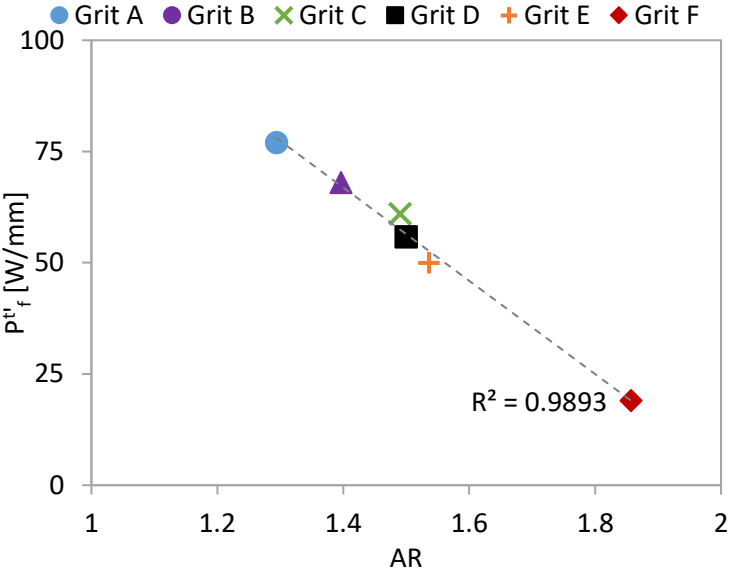

Figure 21: Correlation between specific threshold power and grit shape (AR) (Adopted from Paper III).

The grinding output from Figure 20, is presented in dependence of two grinding inputs Q' (Figure 22) and h_m (Figure 23). The total specific grinding energy in the graphs, (u_e), which unlike the u_e^*, gives the combined information regarding the cutting and rubbing energy. The results on Figure 22 are suggesting that the u_e is grit-shape dependent. On the other hand, Figure 23 shows that at the particular h_m, the u_e remains unchanged regardless of the grit shape. The conclusion that can be drawn for these trials is that the contact area and h_m are grit shape dependent.
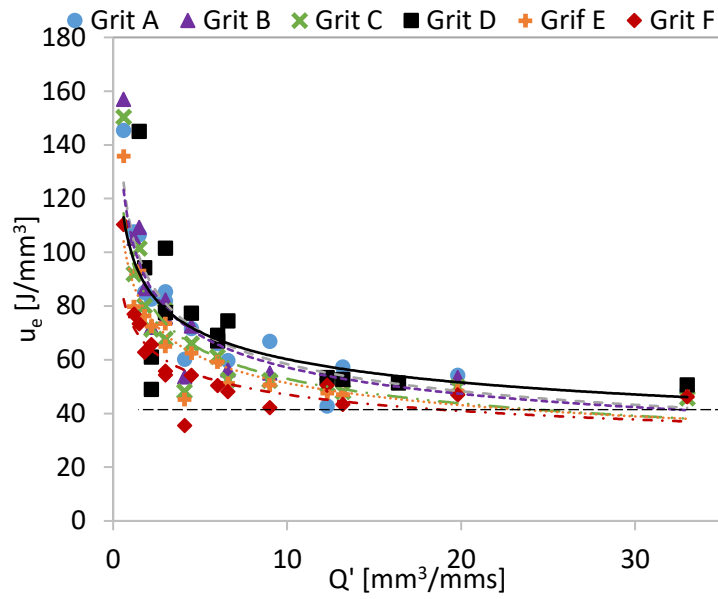
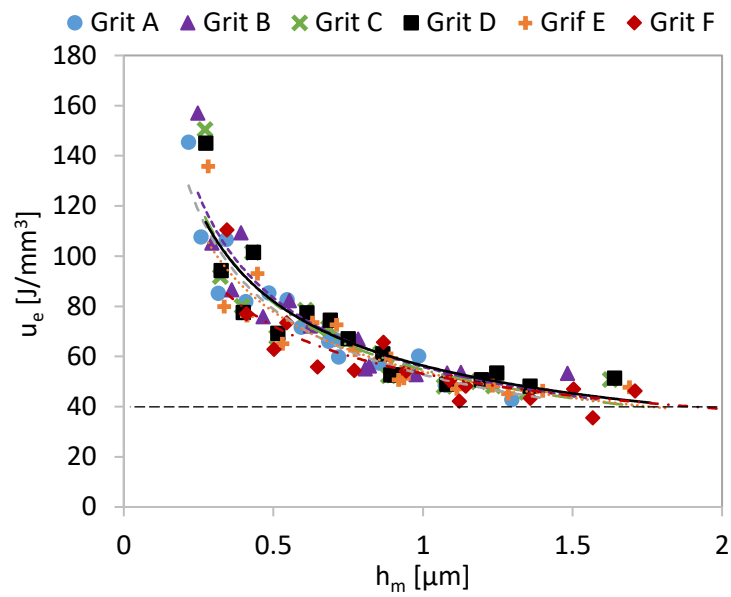*Figure 22: Correlation between u_e and Q'.*

Figure 23: Correlation between u_e and h_m.

Wear trials were carried out at a constant Q' (Table 3) for a set volume of workpiece ground. Grinding forces were measured in situ. The typical power response is presented in Figure 24. Immediately after dressing there is a high surge in power that reduces rapidly until it stabilizes and maintains the level relatively consistently throughout the test.

26

Table 3: Grinding parameters for micro wear test.

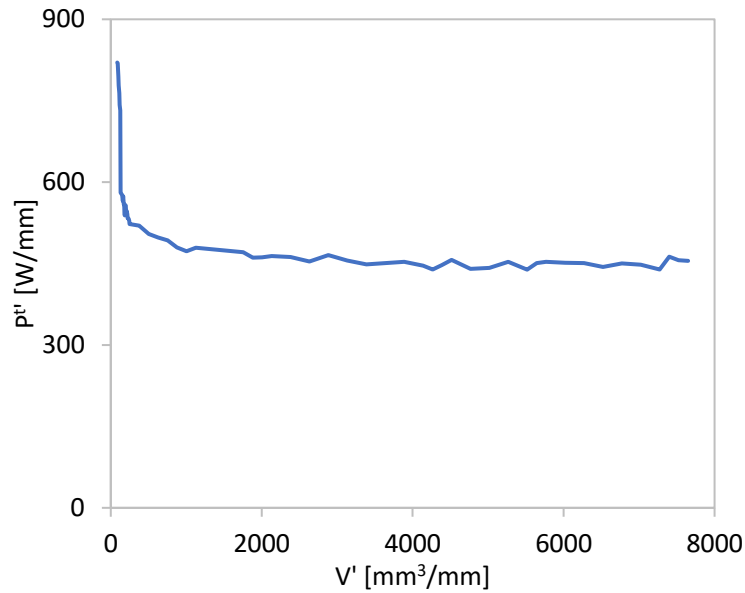|	
Wheel speed, v_s	40 m/s
Depth of cut, a_e	0.033 mm
Workpiece feed rate, v_w	24 m/min
Specific material removal rate, Q'	13.2 mm^3/mms

Figure 24: Typical power response in micro wear test.

The average stabilized power ($P^{t'}$) and normal force ($F^{n'}$) were extracted from results for each grit type and plotted against the grit shape (Figure 25 and Figure 26). There is a relatively good correlation between $P^{t'}$ and grit AR, i.e. the grit with higher AR (elongated) generates lower power and vice-versa (Figure 25). Similar trend is observed also for the normal force (Figure 26). Notice, two grinding wheels that consist of Grit C and Grit D deviate from the trend by generating higher normal forces.
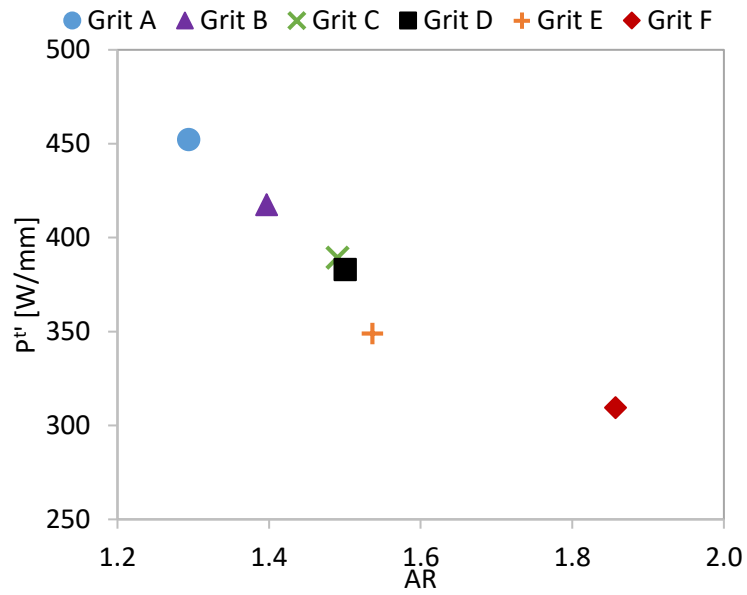
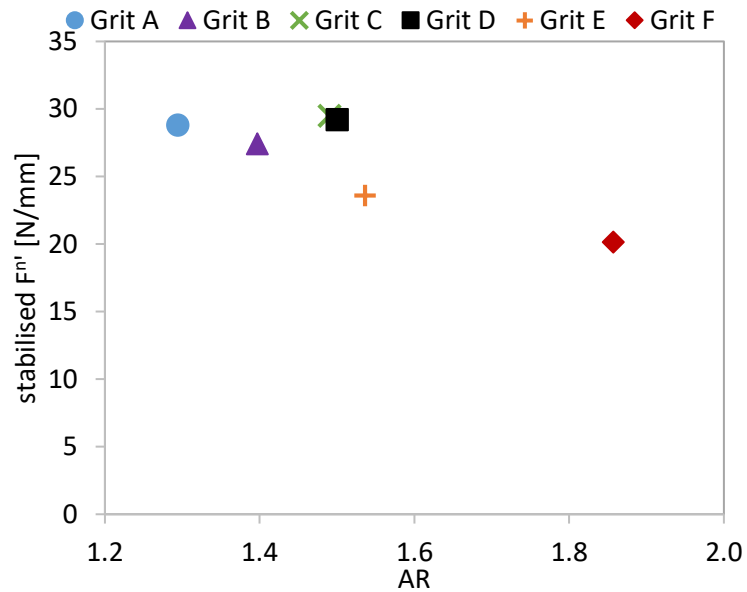*Figure 25: Correlation between power and aspect ratio of grit.*

Figure 26: Correlation between the $F^{n'}$ and the AR of grit.

The grinding wheel wear exhibited on Figure 27 is a reflection of the Figure 26. The general trend is that a grit with lower *AR* generates higher forces and consequently lower grinding wheel wear. The two grit types (Grit C and Grit D) that generated particularly high $F^{n'}$ result in even lower wheel wear.
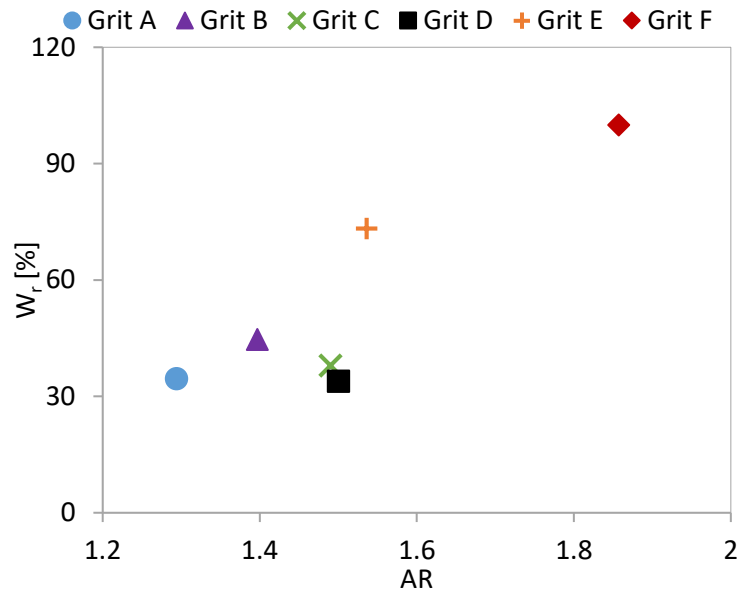
Figure 27: Correlation between the wheel wear and the aspect ratio of grit.

There are a few potential reasons for observed behavior of Grit C and Grit D. The reasons could be related to dressing ability of these particular types. Based on grinding forces, the behavior just after dressing does not indicate abnormal behavior. Another reason could be differences in surface determination of the two grit types, affecting the adhesion of the grit in the bond. Even though these properties have not been evaluated, the cause could be eliminated based on the fact that it is not the only grain coming from a particular synthesis process. Alternative reasons could be in the overall grinding wheel behavior. There might be workpiece adhesion or wheel loading causing performance deviations. The wheel surface has not been analyzed after the test, thus the latter assumptions could not be confirmed.

3.4.2 Performance evaluation of grit concentration variation

The concentration of the grinding wheel is defined by the amount of cBN particles in a particular volume of bond. A standard rule says that 4.4 carats of cBN contained in a volume of $1cm^3$ of material equates to concentration of 100.

High concentration grinding wheels are very common in applications where the contact between the grinding wheel and the workpiece is relatively low (e.g. cylindrical grinding). A higher number of effective grains causes more heat leading to thermal damage. By keeping the contact lengths l_c the likelihood can be minimized and the benefits of extended tool life can emerge.

29

Two different concentrations were evaluated with high concentrations more common for cylindrical grinding applications. Based on experiences, the wheel manufacturer considers the concentration differences to be meaningful. ABN800 has been used in both wheels. The material comes from one batch and has the same AR and strength.

The grinding parameters, for window of operation test are summarized Table 4.

Table 4: Grinding parameters for window of operation test.

Wheel speed, v_s	40 m/s
Depth of cut, a_e	0.01 - 0.3 mm
Workpiece feed rate, v_w	1.2 - 24.6 m/min
Specific material removal rate, Q'	0.6 - 33 mm^3/mms

The results of window of operation tests are illustrated in Figure 28. A noticeable difference in intrinsic specific grinding energy (u_e^*) is observed. A higher trend line inclination can be observed for the higher concentration wheel.

Both grinding wheels have equal amount of porosity and bond and variable amount of cBN. In order to substitute the missing cBN in lower concentration wheel, secondary abrasives are utilized. The difference in u_e^* suggests that the lower concentration wheel acts sharper due to smaller amount of cBN particles. The specific threshold power measurements ($P_f^{t'}$) are higher for higher concentration wheel. This can be directly related to the higher amount of cBN particles per unit area generating higher contact area with the workpiece.
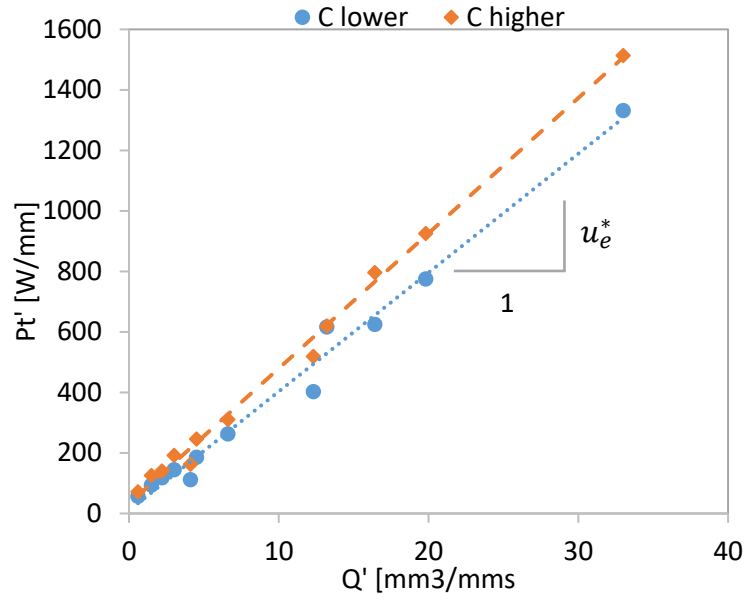
Figure 28: Window of operation results for two different grit concentrations.

Two sets of grinding parameters were used for evaluation of the wear of the two grinding wheels (Table 5). They have suitable low depth of cut to ensure low contact length common for high concentration grinding wheels. The h_m generated from this processes are expected to be short and thick as expected in cylindrical and surface grinding.

Table 5: Grinding parameters for micro wear test.

	Parameters A	Parameters B
Wheel speed, v_s	70 m/s	70 m/s
Depth of cut, a_e	0.04 mm	0.04 mm
Workpiece feed rate, v_w	12 m/min	25 m/min
Specific material removal rate, Q'	8 mm^3/mms	16.7 mm^3/mms

The forces generated using Parameters A (Table 5) are shown in Figure 29. A slow increase in normal ($F^{n\prime}$) and tangential ($F^{t\prime}$) force component can be observed. This suggests that the grit is either dulling, the wheel is loading with the workpiece material or there is adhesion of the workpiece on the wheel. The same trend can be observed for both wheel concentration.
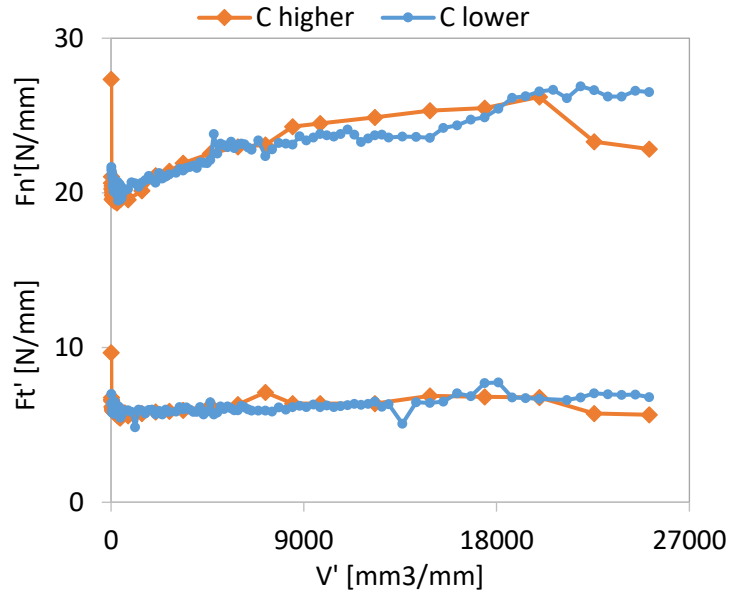
31

Figure 29: Grinding forces generated when grinding with parameters A.

Identical test was done using Parameters B (Table 5). The results are presented in Figure 30. In this case, the grinding forces are not increasing, suggesting the self-sharpening process is taking place preventing grit dulling. The difference between the two wheels are almost negligible.
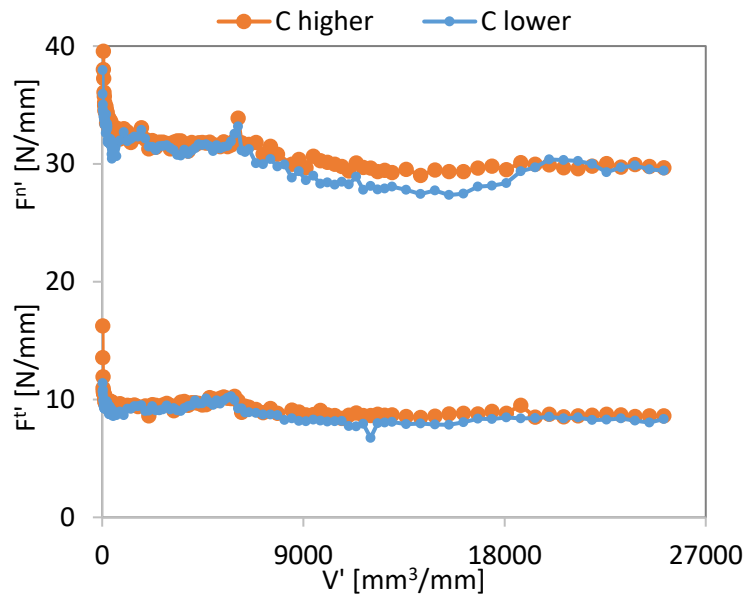

Figure 30: Grinding forces generated when grinding with Parameters B.

Grinding wheel progression was monitored throughout the testing. A significant amount of material was ground and less than 10 µm wear was generated. The wear levels are comparable to those in the real applications. The first observation is that it is not possible to distinguish between the wear of the two wheel concentrations when grinding at lower Q' (Figure 31, a).

32

This might be a result of grit rubbing being a dominant wear mode which was suggested also based on the analysis of force trends (Figure 29). The difference in wear becomes more prominent when grinding with higher Q' (Table 5). Here the lower concentration wheel wears more (Figure 31, b). The higher concentration grinding wheel shows comparable wear level to the first grinding test.
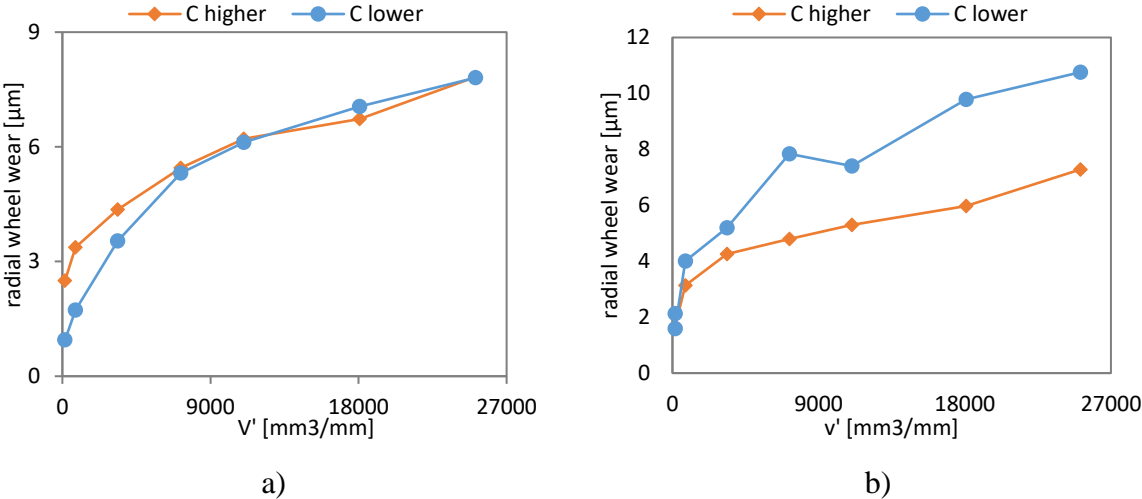

Figure 31: Grinding wheel wear when grinding with: a) Parameters A and b) Parameters B.

Surface roughness was also measured throughout the test. The results are shown on Figure 32. Similarly to the wear measurements where little difference could be observed for lower Q' (Figure 31, a) the roughness measurements do not show significant discrimination between lower and higher concentration grinding wheel (Figure 32, a). On the other hand, significant differences can be observed when grinding at higher Q' (Figure 32, b). The grinding wheel with higher concentration generates superior surface finish and vice versa.
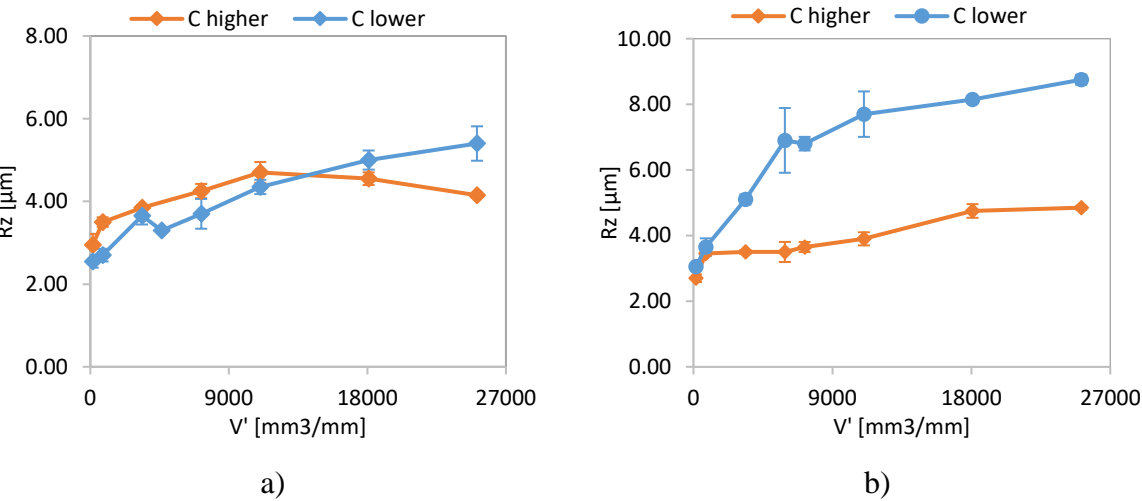

Figure 32: Surface roughness when grinding with a) Parameters A and b) Parameters B.

Higher concentration of cBN has higher number of particles per area. More particles are doing the same amount of work (at the same Q') reducing the h_m and also force per particle. The consequence is reduced grinding wheel wear, confirmed by grinding trials. Equally the increased number of effective edges in the grinding process improves the surface finish.

4   Summary and future work

The work presented in this thesis has generated valuable knowledge on how the grit shape and concentration affect the grinding performance. It was confirmed that grit with lower *AR* (blockier) generates higher forces and increased tool life. Similar behavior was exhibited by higher grit concentration. On the other hand the grit with higher *AR* (elongated) and the lower concentration wheels acted more free-cutting. The continuation of the project proposes following future work:

(i)   Evaluate the performance of the grit strength, shape and size in the same bond formation in a lab-based environment.

(ii) Based on findings from the thesis prepare variations of wheels and test on the newly developed crankshaft grinding strategy. Correlate findings with the lab-based results.

(iii) Evaluate grinding wheel wear from the crankshaft grinding application and correlate with findings from the thesis.

(iv) Propose a grinding wheel wear model using experimental data from the lab and production-based trials.

(v)   Based on the performance of first iteration of grinding wheel propose the next solution, leading to a new generation of multi-grit cBN grinding wheel for crankshaft grinding.

5 Acknowledgements

6 References

[1] J.F.G. Oliveira, E.J. Silva, J.J.F. Gomes, F. Klocke, D. Friedrich. Analysis of Grinding Strategies Applied to Crankshaft Manufacturing. CIRP Ann. - Manuf. Technol. 2005; 54 (2): 269–272.

[2] R. Dražumerič, R. Roininen, J. Badger, P. Krajnik. Temperature-Based Method for Determination of Feed Increments in Crankshaft Grinding. J. Mater. Process. Technol. 2018; 259: 228–234.

[3] P. Krajnik, R. Roininen, R. Drazumeric. Method of grinding a workpiece having a cylindircal bearing surface and method for determining processing parameters, EP3115149B1, 2018.

[4] S. Malkin, C. Guo. Grinding Technology: Theory and Applications of Machining with Abrasives, 2nd ed., 2008.

[5] P. Krajnik, R. Drazumeric, J. Badger, F. Hashimoto. Cycle Optimization in Cam-Lobe Grinding for High Productivity. CIRP Ann. 2014; 63 (1): 333–336.

[6] I. Suzuki, Y. Oda. Method of grinding a workpiece having a cylindrical portion and shoulder portions, 4603514, 1986.

[7] D.A. Mavro-Michaelis. Workpiece grinding method which achieves a constant stock removal rate, US 2005/0032466 A1, 2005.

[8] N. Hori, K. Tabuchi, M. Katsuta, Y. Ito. Workpiece grinding method, US 7,118,453 B2, 2006.

[9] S. Soma, H. Morita. Grindnig method and grinding machine, US 7,530,882 B2, 2009.

[10] M. Banks, E.R. Randell, D.W. Hall, C.D. Bartlett, S. Clewes. Improvements in and relating to the grinding of cylindrical surfaces and adjoining side-walls, 2007.

[11] P. Krajnik, R. Drazumeric, J. Badger, R. Roininen. High-Performance Industrial Grinding: Recent Advances and Case Studies from the Automotive Engine Production, in: Proc. 19th Int. Symp. Adv. Abras. Technol., 2016: pp. 1–13.

[12] J.C. Jaeger. Moving sources of heat and the temperature at sliding contacts, in: Proc. R. Soc. New South Wales, 1942: pp. 203–224.

[13] R. Drazumeric, J. Badger, P. Krajnik. Thermal aspects and grinding aggressiveness in view of optimizing high-performance grinding operations in the automotive industry, in: Proc. ASME Manuf. Sci. Eng. Conf., 2014: pp. 1–7.

[14] P. Comley, I. Walton, T. Jin, D.J. Stephenson. A High Material Removal Rate Grinding Process for the Production of Automotive Crankshafts. CIRP Ann. - Manuf. Technol.

2006; 55: 347–350.

[15] M.J. Jackson, C.J. Davis, M.P. Hitchiner, B. Mills. High-Speed Grinding with CBN Grinding Wheels — Applications and Future Technology. J. Mater. Process. Technol. 2001; 110 (1): 78–88.

[16] J. Webster, M. Tricard. Innovations in Abrasive Products for Precision Grinding. CIRP Ann. 2004; 53 (2): 597–617.

[17] J. Yang, D.-Y. Kim, H.-Y. Kim. Effect of Glass Composition on the Strength of Vitreous Bonded C-BN Grinding Wheels. Ceram. Int. 1993; 19 (2): 87–92.

[18] D. Shan, Z. Li, Y. Zhu, H. Ye, K. Gao, Y. Yu. Influence of TiO2 on the Physical Properties of Low-Temperature Ceramic Vitrified Bond and Mechanical Properties of CBN Composites. Ceram. Int. 2012; 38 (6): 4573–4578.

[19] J. Shi, F. He, J. Xie, X. Liu, H. Yang. Effect of Heat Treatments on the Li2O-Al2O3-SiO2-B2O3-BaO Glass-Ceramic Bond and the Glass-Ceramic Bond CBN Grinding Tools. Int. J. Refract. Met. Hard Mater. 2019; 78: 201–209.

[20] X. Wang, T. Yu, X. Sun, Z. Wang, W. Wang. Effects of ZrO2 on Physical and Mechanical Properties of Vitrified Bond CBN Composite Materials. J. Ceram. Process. Res. 2016; 17 (9): 969–973.

[21] R. Cai, W.B. Rowe, M.N. Morgan. The Effect of Porosity on the Grinding Performance of Vitrified CBN Wheels. Key Eng. Mater. - KEY ENG MAT 2003; 238: 295--300.

[22] X. Lv, Z. Li, Y. Zhu, J. Zhao, G. Zhao. Effect of PMMA Pore Former on Microstructure and Mechanical Properties of Vitrified Bond CBN Grinding Wheels. Ceram. Int. 2013; 39 (2): 1893–1899.

[23] T. Tanaka, S. Edaki, T. Nishida, T. Nakajima, K. Ueno. Development and Application of Porous Vitrified-Bonded Wheel with UltraFine Diamond Abrasives. Key Eng. Mater. - KEY ENG MAT 2004; 257–258: 251–256.

[24] J.B. Mao, F.L. Zhang, G.C. Liao, Y.M. Zhou, H.P. Huang, C.Y. Wang, S.H. Wu. Effect of Granulated Sugar as Pore Former on the Microstructure and Mechanical Properties of the Vitrified Bond Cubic Boron Nitride Grinding Wheels. Mater. Des. 2014; 60: 328–333.

[25] X. Lv, Z. Li, Y. Zhu, J. Zhao, G. Zhao. Effect of PMMA Pore Former on Microstructure and Mechanical Properties of Vitrified Bond CBN Grinding Wheels. Ceram. Int. 2013; 39 (2): 1893–1899.

[26] T.D. Davis, J. DiCorleto, D. Sheldon, J. Vecchiarelli, C. Erkey. A Route to Highly Porous Grinding Wheels by Selective Extraction of Pore Inducers with Dense Carbon

Dioxide. J. Supercrit. Fluids 2004; 30 (3): 349–358.

[27] W.F. Ding, J.H. Xu, Z.Z. Chen, C.Y. Yang, C.J. Song, Y.C. Fu. Fabrication and Performance of Porous Metal-Bonded CBN Grinding Wheels Using Alumina Bubble Particles as Pore-Forming Agents. Int. J. Adv. Manuf. Technol. 2013; 67 (5–8): 1309–1315.

[28] R.H. Wentorf. Abrasive material and preparation thereof, US2947617, 1960.

[29] B.A. Cooley. Superhard Abrasive Developments from De Beers, in: Int. Congr. Diamonds Ind., 1976: pp. 17–29.

[30] O. Fukunaga, S. Nakano, T. Taniguchi. Nucleation and Growth of Cubic Boron Nitride Using a Ca-B-N Solvent. Diam. Relat. Mater. 2004; 13 (9): 1709–1713.

[31] G. Davies. Materials sythesis- internal report, 2014.

[32] T. Taniguchi, S. Yamaoka. Spontaneous Nucleation of Cubic Boron Nitride Single Crystal by Temperature Gradient Method under High Pressure. 2001; 222: 549–557.

[33] T. Taniguchi, S. Koizumi, K. Watanabe, I. Sakaguchi, T. Sekiguchi. High Pressure Synthesis of UV-Light Emitting Cubic Boron Nitride Single Crystals. 2003; 12: 1098–1102.

[34] T. Taniguchi, K. Watanabe. Synthesis of High-Purity Boron Nitride Single Crystals under High Pressure by Using Ba – BN Solvent. 2007; 303: 525–529.

[35] Y. Kubota, T. Taniguchi. Synthesis of Cubic Boron Nitride Using Ni-Mo Alloy as a Solvent. Jpn. J. Appl. Phys. 2008; 47 (11): 8375–8378.

[36] W. Guo, X. Jia, W.L. Guo, H.W. Xu, J. Shang, H.A. Ma. Effects of Additive LiF on the Synthesis of CBN in the System of Li3N–hBN at HPHT. Diam. Relat. Mater. 2010; 19 (10): 1296–1299.

[37] Y. Du, T. Zhang. Synthesis of Black CBN Single Crystal in HBN-Li3N-B System. Cailiao Yanjiu Xuebao/Chinese J. Mater. Res. 2007; 21 (6): 669–672.

[38] K. Breder, N. Corbin, P. Chinnakaruppan, S. Hartline. The influence of grinding conditions on the performance of different CBN types, in: Ind. Diam. Rev., 2005: pp. 4–7.

[39] Y. Ichida, M. Fujimoto, Y. Inoue, K. Matsui. Development of a High Performance Vitrified Grinding Wheel Using Ultrafine-Crystalline CBN Abrasive Grains. J. Adv. Mech. Des. Syst. Manuf. 2010; 4 (5): 1005–1014.

[40] B. Zhao, W. Ding, Y. Zhou, H. Su, J. Xu. Effect of Grain Wear on Material Removal Behaviour during Grinding of Ti-6Al-4V Titanium Alloy with Single Aggregated CBN Grain. Ceram. Int. 2019; 45 (12): 14842–14850.

[41] Z. Rao, W. Ding, Y. Zhu, H. Su. Understanding the Self-Sharpening Characteristics of Polycrystalline Cubic Boron Nitride Super-Abrasive in High-Speed Grinding of Inconel 718. Ceram. Int. 2019; 45 (10): 13324–13333.

[42] Y. Zhu, W. Ding, Z. Rao, C. Yang. Micro-Fracture Mechanism of Polycrystalline CBN Grain during Single Grain Scratching Tests Based on Fractal Dimension Analysis. Precis. Eng. 2019; 59: 26–36.

[43] N.G. Belling, H.G. Dyer. Impact Strength Determination of Diamond Abrasive Grit. Ind. Diam. Inf. Bur. 1964; 1–12.

[44] Y. Chen, X. Chen, L. Aiouarab, T. Opoz, X.P. Xu, G. Yu. Morphology Analysis and Characteristics Evaluation of Typical Super Abrasive Grits in Micron Scale. J. Superhard Mater. 2019; 41 (3): 189–200.

[45] M.W. Bailey, L.K. Hedges. Crystal morphology identification of diamond and ABN, in: Ind. Diam. Rev., 1995: pp. 11–14.

[46] M.P. Hitchiner, S.B. Mcspadden. Evaluation of Factors Controlling CBN Abrasive Selection for Vitrified Bonded Wheels. CIRP Ann. - Manuf. Technol. 2005; (3): 3–6.

[47] R.P. Upadhyaya, J.H. Fiecoat. Factors Affecting Grinding Performance with Electroplated CBN Wheels. CIRP Ann. - Manuf. Technol. 2007; 56 (1): 339–342.

[48] D. Egan. Level Zero: Coatings -Internal Report. 2011; .

[49] M.J. Jackson, B. Mills, M.P. Hitchiner. Controlled wear of vitrified abrasive materials for precision grinding applications, in: Sadhana Acad. Proc. Eng. Sci., 2003: pp. 897–914.

[50] S. Malkin, N.K. Cook. The Wear of Grinding Wheels: Part 1—attritious Wear. ASME. J. Eng. Ind. 1971; 93 (4): 1120–1128.

[51] S.S. Malkin, N.H. Cook. The Wear of Grinding Wheels: Part 2—Fracture Wear. ASME. J. Eng. Ind. 1971; 93 (4): 1129–1133.

[52] M.W. Bailey, H.O. Juchem. The advantages of cBN grinding : low cutting forces and improved workpiece integrity, in: Ind. Diam. Rev., 1998: pp. 89–89.

[53] T.T. Öpöz, X. Chen. Experimental Investigation of Material Removal Mechanism in Single Grit Grinding. Int. J. Mach. Tools Manuf. 2012; 63: 32–40.

[54] Y. Zhu, W. Ding, Z. Rao, C. Yang. Micro-Fracture Mechanism of Polycrystalline CBN Grain during Single Grain Scratching Tests Based on Fractal Dimension Analysis. Precis. Eng. 2019; 59: 26–36.

[55] B. Zhao, W. Ding, Y. Zhou, H. Su, J. Xu. Effect of Grain Wear on Material Removal Behaviour during Grinding of Ti-6Al-4V Titanium Alloy with Single Aggregated CBN

Grain. Ceram. Int. 2019; 45 (12): 14842–14850.

[56] X. Huang, H. Li, Z. Rao, W. Ding. Fracture Behavior and Self-Sharpening Mechanisms of Polycrystalline Cubic Boron Nitride in Grinding Based on Cohesive Element Method. Chinese J. Aeronaut. 2018; .

[57] M. O'Dwyer. Internal Friatest Procedure. 2014; 1–8.

[58] M. Mostofi. Drilling Repsponse of impregnated diamond bits: modelling and experimental investigation, Curtin University, 2014.

[59] S. Agarwal, P. Venkateswara Rao. Predictive Modeling of Undeformed Chip Thickness in Ceramic Grinding. Int. J. Mach. Tools Manuf. 2012; 56: 59–68.

[60] P.V. Vinay, C.S. Rao. Grinding Mechanics and Advances - A Review. J. Mech. Eng. Technol. 2013; 5 (2): 41–74.

[61] S. Malkin. Specific Energy and Mechanisms in Abrasive Processes, in: Third North Am. Metalwork. Res. Conf., Carnegie Press, Pittsburgh, 1975: pp. 453–465.

[62] E. Detournay, P. Defourny. A Phenomenological Model for the Drilling Action of Drag Bits. Int. J. Rock Mech. Min. Sci. Geomech. Abstr. 1992; 29 (1): 13–23.